IJST, Transactions of Electrical Engineering, Vol. 35, No. E1, pp 1-11
Printed in The Islamic Republic of Iran, 2011

STUDY OF THE CONDUCTION BAND OFFSET ALIGNMENT CAUSED BY OXYGEN VACANCIES IN SIO2 LAYER AND ITS EFFECTS ON THE GATE LEAKAGE CURRENT IN NANO-MOSFETS*

LING-FENG MAO

School of Urban Rail Transportation, 178 Gan-jiang East Road, Soochow University, Suzhou 215006, People's Republic of China
Email: mail_lingfeng@yahoo.com.cn

Abstract– The effects of the oxygen vacancies on the microscopic potential distribution and macroscopic potential averaged over one period around the defect for silicon dioxide have been investigated via first-principles calculations. The results demonstrate that such an effect is limited to the dimensions of one cell. Detailed analysis of the planar macroscopic average potential shows that the conduction band alignment caused by the defect and its effects on the tunneling currents have been calculated. The calculations demonstrate that the relative increase in the electron direct tunneling current caused by the oxygen vacancy depends on the position of oxygen vacancy. It is also shown that the increase in the direct tunneling current caused by the oxygen vacancy exponentially decreases with increasing oxide thickness, whereas its relative increase changes little.

Keywords– Dielectric films, MOSFETs, silicon dioxide, tunneling

1. INTRODUCTION

It is widely believed that SiO_2 is approaching its physical limit due to its high leakage current when the dimension-scaling continues to shrink the thickness of the gate dielectrics in a transistor down to nanometers. Now the silicon oxynitride and high-k dielectric have been extensively used as the gate dielectric. However, silica still plays an important roll as an interlayer between the channel and the high-k gate dielectric, and it is almost impossible to effectively grow HfO_2 on Si without the formation of an interfacial SiO_2 or silicate-like layer. Structure defects in crystalline and amorphous silica play an important role in the performance of microelectronics devices. A major concern in silicon technology is the reliability of MOSFETs (metal-oxide-semiconductor field effect transistor) while they are scaled to nanometers. As scaling trends shrink the thickness of the gate dielectrics in transistors, silica will likely fail to meet the industry requirements of an insulating barrier due to defect-mediated leakage and quantum-mechanical tunneling current. The point defects in silica will result in the localized states being introduced into the band gap of silica. They are potential sources of the leakage current in MOSFET. A large number of experimental and theoretical studies have been devoted to the characterization of the point defects in silica due to their role in the degradation of silica based electronic devices [1-15].

The simplest, but also most important defect in SiO_2 is the oxygen vacancy corresponding to the process: ≡Si—O—Si≡ → ≡Si—Si≡ +O; two Si—O bonds are broken and replaced by a single Si—Si bond. The bond angle between O-Si-O is always 109^o while the bond angle between Si-O-Si ranges from 120^o to 180^o. The bond will be severely weakened above 150^o and can lead to bond breakage, followed by the oxygen vacancy, which comes after bond breakage. A complex of a hydrogen atom with an oxygen

*Received by the editors April 28, 2010; Accepted May 21, 2011.

vacancy has been reported as the defect responsible for stress induced leakage current [4]. The neutral oxygen vacancies were believed to cause an optical absorption band with a maximum at around 7.6 eV in both crystalline quartz and in amorphous SiO_2 [5].

In this work, first-principles simulations have been used to study how the oxygen vacancies affect the planar microscopic potential around oxygen vacancies. Thus the conduction band alignment around the vacancy is estimated. Finally, we analyze how the oxygen vacancies in the oxide affect the tunneling current through the oxide in a MOSFET.

2. METHODS

Amorphous silicon dioxide is believed to have similar band structure properties to those of alpha quartz, and the techniques used for determining the behavior of alpha quartz have also been applied to the more disordered structure of silicon dioxide [16]. The plane wave pseudopotential method within density functional theory under the Perdew-Burke-Ernzerh generalized-gradient approximation was used to calculate the total energy and electron structure [17]. Pseudo-wave-functions were expanded in plane waves, and the Brillouin zone was sampled by a Monkhorst- Pack mesh. By using Broyden-Fletcher-Goldfarb-Shanno update scheme, structural and electronic parameters of the relaxed structure can be obtained [17]. CASTEP software has been used in this paper. In this work, Pseudo-wave-functions were expanded in plane waves up to a kinetic energy cutoff of 260 eV, and the Brillouin zone was sampled by a Monkhorst- Pack mesh of k points, with a k-point spacing of 0.04Å^{-1}. Structural and electronic parameters of relaxed structure were performed using Broyden-Fletcher-Goldfarb-Shanno update scheme until the max force on the atoms was less than 0.1 eV/Å.

In order to determine the valence band alignment in the first-principles calculations [18-20], the local potentials have been calculated. This means that a planar microscopic potential along the z direction $\overline{V}_{tot}(z)$ can be obtained based on the local potential. Thus a planar macroscopic potential $\overline{\overline{V}}_{tot}(z)$ averaged over one period can be obtained as

$$\overline{\overline{V}}_{tot}(z) = \frac{1}{L}\int_{z-L/2}^{z+L/2}\overline{V}_{tot}(z')dz' \tag{1}$$

where L is the length of a single period. Therefore the potential shift $\Delta\overline{\overline{V}}_{tot}$ can be used to determine the valence band offset [18-20]:

$$\Delta E_v = \Delta\overline{\overline{V}}_{tot} + \Delta E_{VBM} \tag{2}$$

where ΔE_{VBM} is the difference in the energies of valence band maxima of the two bulk materials measured with respect to their respective bulk potentials.

The direct tunneling current has been calculated by using the following equation [21]:

$$J = \int_0^\infty \frac{qm_z^*}{2\pi^2\hbar^3}T(E_z)\left(\int_{E_z}^\infty [f_r(E) - f_l(E)]dE\right)dE_z \tag{3}$$

where $T(E_z)$ is the transmission coefficient when the longitudinal electron energy is E_z, and f_r and f_l are the distribution functions in the right and the left contact. The transmission coefficient $T(E)$ has been calculated by a numerical solution to the one-dimensional Schrödinger equation under effective mass approximation. The barrier has been discretized by N partial subbarriers of rectangular shape covering the gate oxide. From the continuity of wave function and quantum current density at each boundary, the transmission coefficient is then found by

$$T(E_z)=\frac{m_0}{m_{N+1}}\frac{k_{N+1}}{k_0}\frac{|\det M|}{|M_{22}|^2} \tag{4}$$

where M is a (2×2) product matrix, M_{22} is the quantity of the second row and the second column in this matrix $M=\prod_{l=0}^{N}M_l$ with transfer matrices M_l given by

$$M_l=\frac{1}{2}\begin{vmatrix} (1+S_l)\exp[-i(k_{l+1}-k_l)z_l] & (1-S_l)\exp[-i(k_{l+1}+k_l)z_l] \\ (1-S_l)\exp[+i(k_{l+1}-k_l)z_l] & (1+S_l)\exp[+i(k_{l+1}-k_l)z_l] \end{vmatrix} \tag{5}$$

In the above equation $S_l=m_{l+1}k_l/m_lk_{l+1}$, z_l is the position of the lth boundary, and the effective masses and momenta are discretized as $m_l=m^*[(z_{l-1}+z_l)/2]$ and $k_l=\frac{\sqrt{2m_l\left(E-\phi+q\frac{V_{ox}}{t_{ox}}(z_{l-1}+z_l)/2\right)}}{\hbar}$ (V_{ox} is the applied voltage across the oxide, t_{ox} is the thickness of the oxide, and ϕ is the barrier height), respectively. From the expression of the wave vector, the effect of the barrier height and the voltage on the transmission coefficient can be found. The Fermi-Dirac distribution was used in the tunneling current calculations, in which the maximum of the longitudinal electron energy was set at $20k_BT$ (k_B is Boltzmann constant, T is the temperature) above the conduction band. The entire oxide is assumed to be composed of many supercells, (some with the oxygen vacancy and the others without oxygen vacancies), and thus dilute vacancies can be calculated according to the following expression:

$$J=\frac{1}{S}\int_s j(x,y)ds \tag{6}$$

where S is the area of the oxide, j(x,y) is the local tunneling current. By using the Eq.6, the effects of the oxygen vacancies with arbitrary concentration on the tunneling currents can be calculated. For simplicity, the defect oxide layer has been assumed to be composed of the same supercell with one oxygen vacancy in this work. Compared to first principle calculation of leakage current applying Non-Equilibrium Green's function (NEGF), the above method can exponentially save calculation time.

3. RESULTS AND DISCUSSION

The supercell method with 72 atoms has been used to model defects in quartz [22] and to comparatively study the defect energetics in the monoclinic hafnium oxide and α-quartz [23]. In this work, a sandwich structure, which is the perfect α-quartz supercell layer/the defect α-quartz supercell layer/ the perfect α-quartz supercell layer (the interface is perpendicular to z direction, the structure used in this work has 107 atoms), has been studied by using the first-principles simulations. Every supercell is composed of 2×2×1 α-quartz cell. One oxygen atom in the middle of the oxide layer has been removed and forms a defect layer. The crystal parameters of the α-quartz unit cell used in the simulations have been selected according to reference [24]: a=4.9384, b= 4.9384, c=5.4213. In this work, the x direction and the z direction represent the a-axis and the c-axis of the α-quartz cell, respectively.

Figure 1 shows the contour of the microscopic potential of the plane where the oxygen vacancy locates in the defect oxide layer and the corresponding oxygen site locates in the perfect oxide layer. From these figures, it is clearly seen that the oxygen vacancy will result in a larger change in the microscopic potential around the position of vacancy (the coordinates of the vacancy position are x=2.7 Å and y=2.5 Å,

respectively). Checking Fig. 1, it can be concluded that the change in the microscopic potential distribution of the plane at the position of the oxygen vacancy in the oxide is limited to the dimensions of one cell.

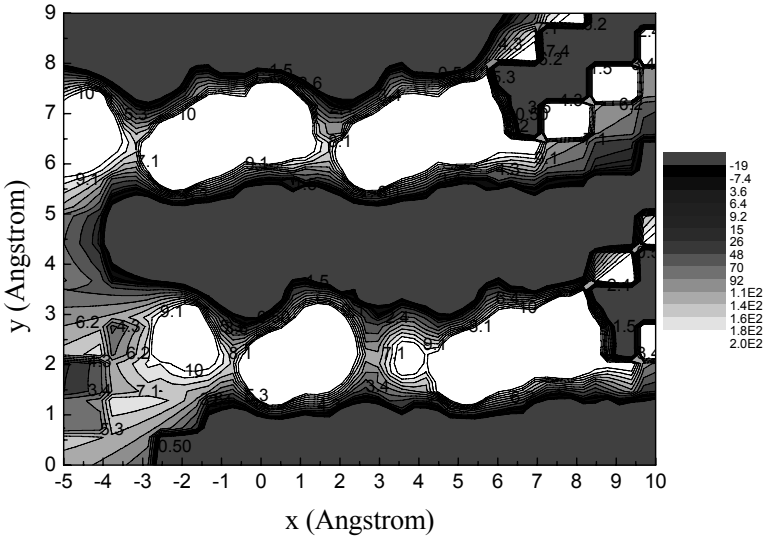

(a)

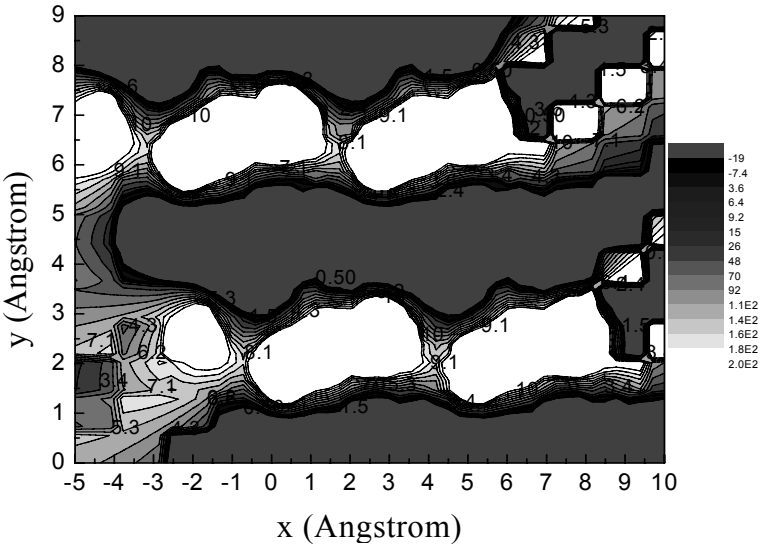

(b)

Fig. 1. The contour of the microscopic potential at the plane where oxygen vacancy locates in the defect oxide layer (a) and the corresponding plane locates in the perfect oxide layer (b)

Figure 2a demonstrates the planar averages microscopic potential along the *z* direction and the macroscopic potential averaged over one period along the *z* direction (the *z* direction is perpendicular to the perfect oxide/ defect oxide interface). It is clearly seen in this figure that the significant change in the planar microscopic potential caused by the oxygen vacancy is limited to one period. Figure 2b shows the planar macroscopic potential averaged over one period and its Gaussian fit. From this figure, the relation

between the change of the planar macroscopic potential averaged over one period caused by the oxygen vacancy and the distance away from the position of the oxygen vacancy can be described by using a Gaussian distribution. In this work, the Gaussian fit curve in Fig.2b uses the following form:

$$\phi - \phi_0 = -1.3 \times \frac{1}{\sqrt{2\pi}} \exp\left(-\frac{(z - z_0)^2}{2} \right) \tag{7}$$

where ϕ and ϕ_0 are the potentials which use the unit of eV, z_0 is the position of the oxygen vacancy along z direction, z is the distance away from the position of the oxygen vacancy (z_0 and z use the unit of angstrom). The maximum depth of the change in the planar macroscopic potential averaged over one period caused by the oxygen vacancy is 0.52 eV, and its full width at half minimum is 2 Å. The Gaussian fit here just gives an analytical description of the band edge around the vacancy necessary. One can use the planar average potential and obtain the exact transmission coefficient.

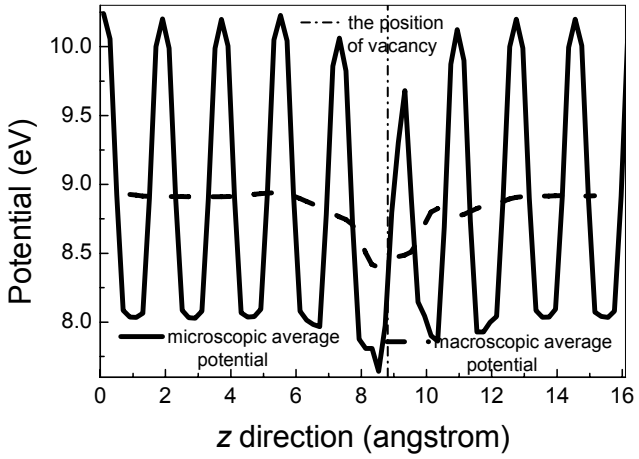

(a)

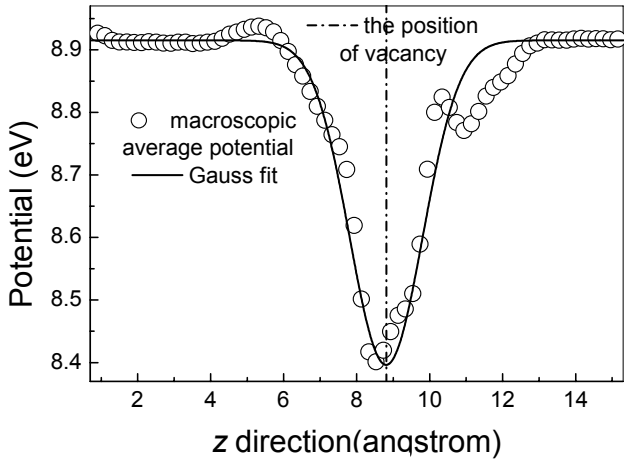

(b)

Fig. 2. The planar averages microscopic potential and the planar macroscopic potential averaged over one period along z direction, which is perpendicular to the perfect oxide/ the defect oxide interface (a); the planar macroscopic potential averaged over one period and its gauss fit (b)

Based on the analysis of the above results, it can be concluded that the length along the *x* direction, the *y* direction, and the *z* direction where the microscopic potential is significantly affected by the oxygen vacancy is limited to one period along the three directions. Thus, the space where the microscopic potential will be affected by the oxygen vacancy can be assumed to be limited to the dimensions of one cell. Therefore, the valid planar macroscopic potential in this case should be averaged over one period, and the effects of the oxygen vacancy on the planar macroscopic potential could be estimated. As we know that the conduction band offset of the heterojunction can be determined by using the planar macroscopic average potential [18-20]. According to the above discussion, this method should also be valid for the case of a perfect α-quartz supercell layer/defect α-quartz supercell layer /perfect α-quartz supercell layer structure after the planar macroscopic potential averaged over one period is valid to describe the effect of the oxygen vacancy on planar macroscopic average potential. For the case of a perfect α-quartz supercell/defect α-quartz supercell/perfect α-quartz supercell structure, ΔE_{VBM} is zero. Thus, Eq. (2) can be rewritten as

$$\Delta E_v = \Delta \overline{\overline{V}}_{tot} \tag{8}$$

Because $\Delta E_g = 0$ in this case (The defect can be assumed not to affect the bandgap), the conduction band offset around the oxygen vacancy can be obtained as

$$\Delta E_c = \Delta \overline{\overline{V}}_{tot} \tag{9}$$

A similar method has been applied to study oxygen vacancies in the conduction band alignment of HfO_2 [25].

Figure 3a shows the conduction band edge profile of an Al/perfect SiO_2/n-Si MOS device when the oxide thickness is 1.5 nm. According to the above discussion, we know that the conduction band alignment around the oxygen vacancy can also be described by using Eq. (7). Figure 3b shows the conduction band edge profile of an Al/defect SiO_2/n-Si MOS device when the oxide thickness is 1.5 nm and the oxygen vacancy locates at the middle of the oxide.

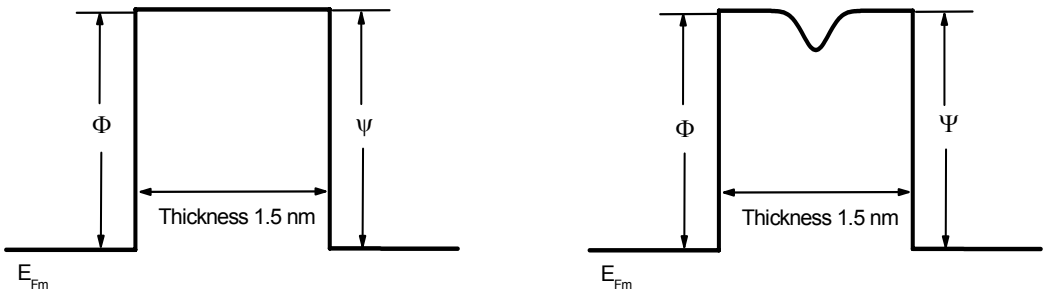

Fig. 3. The conduction band edge profile of an Al/perfect SiO_2/n-Si MOS device (a); the conduction band edge profile of an Al/defect SiO_2/n-Si MOS device with the oxygen vacancy located at the middle of the oxide (b)

The parameters of the effective mass and the barrier height of SiO_2 used in the tunneling current calculations were selected according to Ref. [26] and its corresponding references: the effective electron mass in the oxide is 0.5 m_0 (m_0 is free electron mass) and the barrier height is: $\Phi = 3.17$ eV and $\Psi = 3.15$ eV. The conduction band diagrams, which are shown in Fig. 3, have been used in the following tunneling current calculations.

Figure 4a shows the comparison of the electron direct tunneling current through the perfect oxide and the defect oxide and its relative increase changing with the oxide voltage when the oxide thickness is 1.0 nm, 1.5nm and 2.0 nm, respectively. Here and in the following, J_0 represents the calculated electron tunneling currents though a perfect gate oxide; ΔJ means the increase in the tunneling current caused by the conduction band offset alignment of the gate oxide due to oxygen vacancies compared to that through perfect oxide. From this figure, it is clearly seen that the oxygen vacancy will result in an increase in the electron direct tunneling current. Checking this figure carefully, it can also be concluded that a relative increase in the electron direct tunneling current caused by the oxygen vacancy will increase with increasing oxide voltage but only have a small change with the oxide thickness under the same oxide voltage. Figure 4b shows the comparison of the electron direct tunneling current through the perfect oxide and the defect oxide for different positions of oxygen vacancy. The oxygen vacancy locates in the middle of the oxide, near the gate with the distance between the oxygen vacancy and the gate/oxide interface being 2.9 Å, and near the substrate with the distance between the oxygen vacancy and the substrate/oxide interface being 2.9 Å, respectively. The relative increase in the electron direct tunneling current changing with the oxide voltage is also given in this figure when the oxide thickness is 1.5 nm. It is clearly seen in this figure that it always results in an increase in the electron direct tunneling current through the oxide wherever the oxygen vacancy locates in the oxide. It can also be concluded that the relative increase in the electron direct tunneling current caused by the oxygen vacancy locating near the substrate/oxide interface in the oxide is larger than that of the one locating in the middle of the oxide. It can be noted that the entity of the changes in the tunneling current caused by the alignment of the conduction band offset is rather small. But it does not indicate that the increase in the tunneling current caused by oxygen deficiency does not play a significant role in ultrathin film conduction, as oxygen vacancies can introduce a defect-related energy level within the bandgap and trap-assisted tunneling occurs [27, 28]. Ref. [28] demonstrates that the total relative increase in the leakage current caused by defect assisted electron and hole tunneling varies from 50% to 150% when oxide thickness u changes from 1.5nm to3.0nm at an electric field of 3 MV/cm. Comparing this work with that in Ref. [28], we can find that the increase in the leakage current caused by the defect assisted tunneling is only about 2-3 times that caused by the band offset shift. These indicate that the leakage current caused by the band offset shift for ultra-thin oxide cannot be neglected.

According to the $k_l = \frac{\sqrt{2m_l\left(E-\phi+q\frac{V_{ox}}{t_{ox}}\left(z_{l-1}+z_l\right)/2\right)}}{\hbar}$, the defects near the first interface will have different effects on the wave vector than that near the second interface. Thus, the defects locating at different positions will lead to different transmission, and a difference in the leakage current.

Figure 5 shows the comparison of the increase in the electron direct tunneling current caused by the oxygen vacancy and its relative increase changing with the oxide thickness when the oxide electric field is 0.5 MV/cm and 1.0 MV/cm. It is clearly seen in this figure that the increase in the electron direct tunneling current decreases exponentially with the oxide thickness increasing, but its relative increase has

little change with the oxide thickness. After checking the data carefully, it can be found all the (ΔJ or J vs thickness) curves are smooth. Thus, the ripple in Fig. 5 might be caused by the calculation error in numerical calculations.

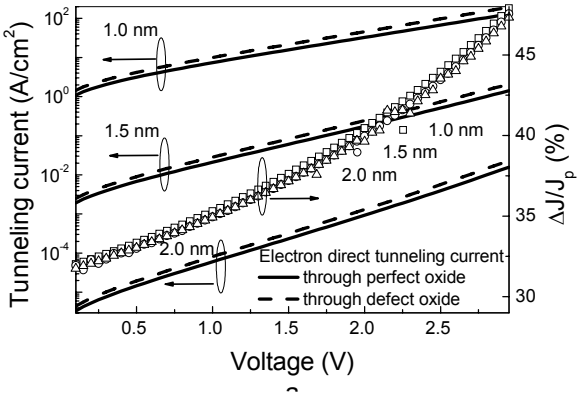

(a)

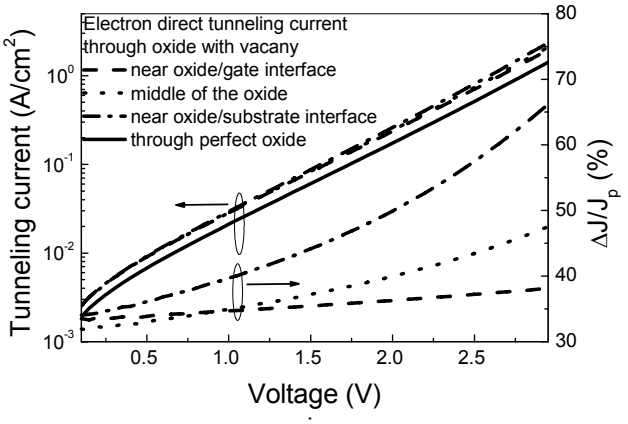

(b)

Fig. 4. The comparison of the electron direct tunneling current through the perfect oxide and the defect oxide and its relative increase changing with the oxide voltage when the oxide thickness is 1.0 nm, 1.5nm and 2.0 nm (a); the comparison of the electron direct tunneling current through the perfect oxide and the defect oxide (the oxygen acancy locates the middle of the oxide, locates the position with the distance between the oxygen vacancy and the gate/oxide interface is 2.9 Å, and locates the position with the distance between the oxygen vacancy and the substrate/oxide interface is 2.9 Å) and its relative increase changing with the oxide voltage when the oxide thickness is 1.5nm (b)

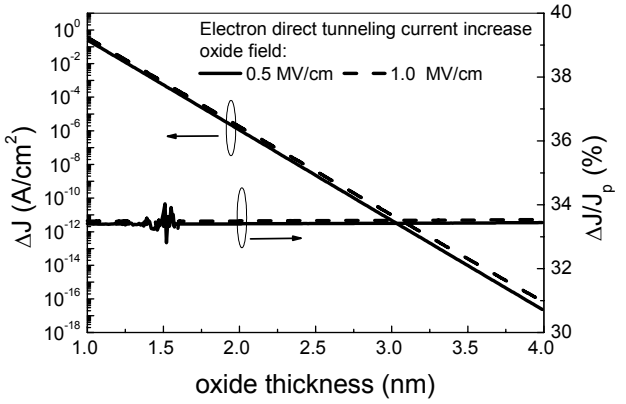

Fig. 5. The comparison of the increase in the electron direct tunneling current caused by the oxygen vacancy and its relative increase changing with oxide thickness when the oxide field is 0.5 MV/cm and 1.0 MV/cm

In a word, the first-principles calculations have been done based on the plane wave pseudopotential method within density functional theory under the Perdew-Burke-Ernzerh generalized-gradient approximation. Such an approximation can lead to underestimation of the band gap and band offsets. In the tunneling current calculation, charge quantization effects at substrate/dielectric interface on the tunneling current have been neglected. There are also some articles on transistors in Iranian Journal of Science and Technology, Transaction B: Engineering [29-30].

4. CONCLUSION

Based on the first-principles calculations, the effects of the oxygen vacancy on the planar microscopic potential and the planar macroscopic potential have been studied. The simulations demonstrate that the oxygen vacancy results in a larger change in the planar microscopic potential around the oxygen vacancy. The planar microscopic potential that will be affected by the oxygen vacancy can be found to be limited to the dimensions of one cell. The planar macroscopic potential has been assumed to be good at studying the oxygen vacancy and its effect on the planar macroscopic potential. The planar macroscopic potential around the oxygen vacancy has been assumed to be as alike as a potential well, with the center being the position of the oxygen vacancy. Detailed analysis demonstrates that the maximum change of the planar macroscopic potential around the oxygen vacancy is 0.52 eV, and its full width at half minimum is 2 Å. Thus, a Gaussian fit is found that can be used to describe the relation between the change in the planar macroscopic potential averaged over one period and the distance away from the position of the oxygen vacancy.

Numerical calculations of the tunneling currents through the ultra-thin SiO_2 layer with or without the oxygen vacancies demonstrate that the oxygen vacancies could result in a large increase in the electron direct tunneling current. Detailed analysis of the results shows that a relative increase in the electron direct tunneling current caused by the conduction band offset alignment will increase with the oxide voltage, but only have a small change with the oxide thickness under the same oxide voltage. The oxygen vacancies can cause an increase in the electron direct tunneling current wherever it locates in the oxide. The relative increase in the electron direct tunneling current caused by the oxygen vacancies depends on its position. The increase in the electron direct tunneling current exponentially decreases with increasing oxide thickness, and the relative increase in the electron tunneling current changes little with the oxide thickness.

***Acknowledgments*:** The author acknowledges financial support from the National Natural Science Foundation of China (NSFC) grant No. 61076102.

REFERENCES

1. Jani, M. G., Bossoli, R. B. & Halliburton, L. E. (1983). Further characterization of the E_1' center in crystalline SiO_2. *Phys Rev. B*, Vol. 27, No. 5, pp. 2285-2293.
2. Martini, M., Paleari, A., Spinolo, G. & Vedda, A. (1995). Role of $[AlO_4]_0$ centers in the 380-nm thermoluminescence of quartz. *Phys Rev. B*, Vol. 52, No. 1, pp. 138-142.
3. Miller, A. J., Leisure, R. G., Mashkov, V. A. & Galeener, F. L. (1996). Dominant role of E′centers in x-ray-induced, visible luminescence in high-purity amorphous silicas. *Phys Rev. B*, Vol. 53, No. 14, pp. R8818-R8820.
4. Blöchl, P. E. & Stathis, J. H. (1999). Hydrogen Electrochemistry and Stress-Induced Leakage Current in Silica. *Phys Rev. Lett.*, Vol. 83, No. 2, pp. 372-375.
5. Skuja, L. (1998). Optically active oxygen-deficiency-related centers in amorphous silicon dioxide. J. *Non-Cryst. Solids*, Vol. 236, No. 1-3, pp. 16-48.

6. Tamura, T., Lu, G. & Yamamoto, R. (2004). First-principles study of neutral oxygen vacancies in amorphous silica and germania. *Phys Rev. B,* Vol. 69, No. 19, pp. 195204-1-195204-1-10.
7. Mukhopadhyay, S., Sushko, P. V., Stoneham, A. M. & Shluger, A. L. (2005). Correlation between the atomic structure, formation energies, and optical absorption of neutral oxygen vacancies in amorphous silica. *Phys Rev. B*, Vol. 71, No. 23, pp. 235204-1-235204-9.
8. Yokozawa, A. & Miyamoto, Y. (1998). First-principles exploration of possible trap terminators in SiO2. *Appl. Phys. lett.*, Vol. 73, No. 8, pp. 1122-1124.
9. Sulimov, V. B., Sushko, P. V., Edwards, A. H., Shluger, A. L. & Stoneham, A. M. (2002). Asymmetry and long-range character of lattice deformation by neutral oxygen vacancy in α-quartz. *Phys Rev. B*, Vol. 66, No. 2, pp. 024108-1-024108-14.
10. Agnello, S., Boscaino, R., Cannas, M., Gelardi, F. M., Leone, M. & Boizot, B. (2003). Competitive relaxation processes of oxygen deficient centers in silica. *Phys Rev. B*, Vol. 67, No. 3, pp. 033202-1-033202-4.
11. Chadi, D. J. (2003). Negative-U property of the oxygen vacancy defect in SiO2 and its implication for the E1′center in α-quartz. *Appl. Phys. lett*., Vol. 83, No.3, pp. 437-439.
12. Mysovsky, A. S., Sushko, P. V., Mukhopadhyay, S., Edwards, A. H. & Shluger, A. L. (2004). Calibration of embedded-cluster method for defect studies in amorphous silica. *Phys Rev. B*, Vol. 69, No. 10, pp. 085202-1-085202-10.
13. Buscarino, G., Agnello, S. & Gelardi, F. M. (2005). Delocalized Nature of the E_δ'Center in Amorphous Silicon Dioxide. *Phys Rev. Lett.*, Vol. 94, No. 12, pp. 125501-1-125501-4.
14. Blöchl, P.E. (2000). First-principles calculations of defects in oxygen-deficient silica exposed to hydrogen, *Phys Rev. B*, Vol. 62, No.10, pp. 6158-6179.
15. Uchino, T., Takahashi, M. & Yoko, T. (2000). Model of oxygen-deficiency-related defects in SiO2 glass. *Phys Rev. B*, Vol. 62, No. 5, pp. 2983-2986.
16. Verwey, J. F., Amerasekera, E. A. & Bisschop, J. (1990). The physics of SiO2 layers. *Rep. Prog. Phys.*, Vol. 53, No.10, pp. 1297-1331.
17. Segall, M. D., Lindan, P. J. D., Probert, M. J., Pickard, C. J., Hasnip, P. J., Clark S. J. & Payne, M. C. (2002). First-principles simulation: ideas, illustrations and the CASTEP code, *J. Phys. Condens. Matter.,* Vol. 14, No.11, pp. 2717-2744.
18. Van der Walle, C. G. & Martin, R. M. (1986). Theoretical calculations of heterojunction discontinuities in the Si/Ge system. *Phys. Rev. B*, Vol. 34, No.8, pp. 5621-5634.
19. Al-Allak, H. M. & Clark, S. J. (2001). Valence-band offset of the lattice-matched β-FeSi2(100)/Si(001) heterostructure. *Phys Rev. B,* Vol. 63, No. 3, pp. 033311-1-033311-4.
20. Puthenkovilakam, R. & Chang, J. P. (2004). Valence band structure and band alignment at the ZrO2/Si interface. *Appl. Phys. lett.*, Vol. 84, No. 8, pp. 1353-1355.
21. Ando, Y. & Itoh, T. (1987).Calculation of transmission tunneling current across arbitrary potential barriers. *J. Appl. Phys.*, Vol. 61, No. 4, pp. 1497-1502.
22. Pickard, C. J. & Mauri, F. (2002). First-Principles Theory of the EPR g Tensor in Solids: Defects in Quartz. *Phys. Rev. Lett.*, Vol. 88, No. 8, pp. 086403-1-086403-4.
23. Scopel, W. L., da Silva, A. J. R., Orellana, W. & Fazzio, A. (2004). Comparative study of defect energetics in HfO2 and SiO2. *Appl. Phys. Lett.*, Vol. 84, No. 9, pp. 1492-1494.
24. Kihara, K. (1990). An X-ray study of the temperature dependence of the quartz structure. *Eur. J. Mineral.*, Vol. 2, No. 1, pp. 63-77.
25. Mao, L. F., Wang, Z. O., Wang, J. Y. & Zhu, C.Y. (2007). The conduction band alignment of HfO2 caused by oxygen vacancies and its effects on the gate leakage current in MOS structures. *Eur. Phys. J. Appl. Phys*., Vol. 40, No. 1, pp. 59-63.

26. Vexler, M. I., Tyaginov, S. E. & Shulekin, A. F. (2005). Determination of the hole effective mass in thin silicon dioxide film by means of an analysis of characteristics of a MOS tunnel emitter transistor. *J. Phys.: Condens. Matter.*, Vol. 17, No. 50, pp. 8057-8068.
27. Mao, L. F. (2007). First-principles study of the effects of oxygen vacancy on hole tunneling current. *Microelectron. Reliab.*, Vol. 47, No. 8, pp. 1213-1217.
28. Mao, L. F. (2007). Tunnelling currents through oxygen vacancies in ultrathin SiO2 layer, *Int. J. Electron.*, Vol. 94, No. 11, pp. 985-994.
29. Saniei, N. & Djahanshahi, H. (2007). A high speed SiGeVCO based on self injection locking scheme. *Iranian Journal of Science & Technology, Transaction B: Engineering*, Vol. 31, No. B6. pp. 641-650.
30. Cheshmehbeigi, H. M. & Afjei, E. (2007). Rotor position detection with employment of the pulse injection technique on switch capacitors in switched reluctance motors. *Iranian Journal of Science & Technology, Transaction B: Engineering*, Vol. 33, No. B2, pp. 149-161.